Supporting Information

Tao E. Li[a], **Joseph E. Subotnik**[a], **and Abraham Nitzan**[a,b]

[a]Department of Chemistry, University of Pennsylvania, Philadelphia, Pennsylvania 19104, USA; [b]School of Chemistry, Tel Aviv University, Tel Aviv 69978, Israel

1. Details on Classical Molecular Dynamics

The quantum Hamiltonian in Eq. (3), although depending only on the nuclear and photonic degrees of freedom, is still too expensive to evolve exactly. The simplest approximation we can make is the classical approximation, i.e., all quantum operators are mapped to the corresponding classical observables, which leads to the following classical Hamiltonian:

$$H^{\rm G}_{\rm QED} = H^{\rm G}_{\rm M} + H^{\rm G}_{\rm F} \tag{S1a}$$

$$H^{\rm G}_{\rm M} = \sum_{n=1}^{N}\left(\sum_{j\in n}\frac{\mathbf{P}^2_{nj}}{2M_{nj}} + V^{(n)}_g(\{\mathbf{R}_{nj}\})\right) + \sum_{n=1}^{N}\sum_{l>n} V^{(nl)}_{\rm inter} \tag{S1b}$$

$$H^{\rm G}_{\rm F} = \sum_{k,\lambda}\frac{\widetilde{p}^2_{k,\lambda}}{2m_{k,\lambda}} + \frac{1}{2}m_{k,\lambda}\omega^2_{k,\lambda}\left(\widetilde{q}_{k,\lambda} + \sum_{n=1}^{N}\frac{d_{ng,\lambda}}{\omega_{k,\lambda}\sqrt{\Omega\epsilon_0 m_{k,\lambda}}}\right)^2 \tag{S1c}$$

Eq. (S1) serves as the starting point of this work. We note that one can go beyond the treatment here by propagating the quantum Hamiltonian Eq. (2) using the path-integral technique (S1, S2) and evolve the ring polymer Hamiltonian with n copies of coupled classical trajectories (aka n beads). In the present manuscript, we focus on the classical system, deferring the path-integral calculation to a later study.

In our classical MD simulations, the simulated system is represented by particles that obey the Newtonian equations of motion:

$$M_{nj}\ddot{\mathbf{R}}_{nj} = \mathbf{F}^{(0)}_{nj} - \sum_{k,\lambda}\left(\varepsilon_{k,\lambda}\widetilde{q}_{k,\lambda} + \frac{\varepsilon^2_{k,\lambda}}{m_{k,\lambda}\omega^2_{k,\lambda}}\sum_{l=1}^{N} d_{lg,\lambda}\right)\frac{\partial d_{ng,\lambda}}{\partial \mathbf{R}_{nj}} \tag{S2a}$$

$$m_{k,\lambda}\ddot{\widetilde{q}}_{k,\lambda} = -m_{k,\lambda}\omega^2_{k,\lambda}\widetilde{q}_{k,\lambda} - \varepsilon_{k,\lambda}\sum_{n=1}^{N} d_{ng,\lambda} \tag{S2b}$$

where the cavity-free force $\mathbf{F}^{(0)}_{nj}$ is calculated by $\mathbf{F}^{(0)}_{nj} = -\partial V^{(n)}_g/\partial\mathbf{R}_{nj} - \sum_{l\neq n}\partial V^{(nl)}_{\rm inter}/\partial\mathbf{R}_{nj}$, and the coupling between particles representing photons and nuclear degrees of freedom is given by $\varepsilon_{k,\lambda} \equiv \sqrt{m_{k,\lambda}\omega^2_{k,\lambda}/\Omega\epsilon_0}$.

Periodic Boundary Condition. A realistic simulation for VSC or V-USC that corresponds to current observations requires a macroscopic number (say, $10^9 \sim 10^{11}$) of molecules (S3–S6), which is far beyond our computational power if we simulate Eq. (S2) directly. To proceed, we assume that the whole molecular ensemble can be divided into $N_{\rm cell}$ periodic cells, in which the molecules evolve identically, i.e., we can approximate the second term on the right of Eq. (S2b) by $\sum_{n=1}^{N} d_{ng,\lambda} = N_{\rm cell}\sum_{n=1}^{N_{\rm sub}} d_{ng,\lambda}$, where $N_{\rm sub} = N/N_{\rm cell}$ denotes the number of molecules in a single cell. By further denoting $\widetilde{\widetilde{q}}_{k,\lambda} = \widetilde{q}_{k,\lambda}/\sqrt{N_{\rm cell}}$, $\widetilde{\widetilde{\varepsilon}}_{k,\lambda} = \sqrt{N_{\rm cell}}\varepsilon_{k,\lambda}$, we can rewrite the equations of motion in Eq. (S2) in a symmetric form

$$M_{nj}\ddot{\mathbf{R}}_{nj} = \mathbf{F}^{(0)}_{nj} - \sum_{k,\lambda}\left(\widetilde{\widetilde{\varepsilon}}_{k,\lambda}\widetilde{\widetilde{q}}_{k,\lambda} + \frac{\widetilde{\widetilde{\varepsilon}}^2_{k,\lambda}}{m_{k,\lambda}\omega^2_{k,\lambda}}\sum_{l=1}^{N_{\rm sub}} d_{lg,\lambda}\right)\frac{\partial d_{ng,\lambda}}{\partial \mathbf{R}_{nj}} \tag{S3a}$$

$$m_{k,\lambda}\ddot{\widetilde{\widetilde{q}}}_{k,\lambda} = -m_{k,\lambda}\omega^2_{k,\lambda}\widetilde{\widetilde{q}}_{k,\lambda} - \widetilde{\widetilde{\varepsilon}}_{k,\lambda}\sum_{n=1}^{N_{\rm sub}} d_{ng,\lambda} \tag{S3b}$$

The form of Eq. (S3) has several advantages. First, we simulate the VSC of a macroscopic number of molecules by evolving molecules in a single cell plus the few photon modes that we are interested in. Second, when considering the dependence of Rabi splitting on molecular numbers, we can fix the number of molecules in a single cell ($N_{\rm sub}$) and vary only the coupling constant $\widetilde{\widetilde{\varepsilon}}_{k,\lambda} = \sqrt{N_{\rm cell}}\varepsilon_{k,\lambda}$. Such a change is very easy to implement in practice and has the physical interpretation of increasing the number of cells while leaving the number of molecules per cell and the size of the simulation cell fixed.

q-TIP4P/F Water Force Field. The question remains as to exactly how we will calculate the ground-state quantities $\mathbf{F}^{(0)}_{nj}$, $d_{ng,\lambda}$, and $\partial d_{ng,\lambda}/\partial\mathbf{R}_{nj}$. In general, these properties can be calculated by classical empirical force field or *ab initio* electronic structure theory. For this initial work, we use an empirical classical force field — the q-TIP4P/F water model (S7) — which provides a simple yet reliable description of both the equilibrium and dynamic properties of liquid water.

www.pnas.org/cgi/doi/10.1073/pnas.2009272117

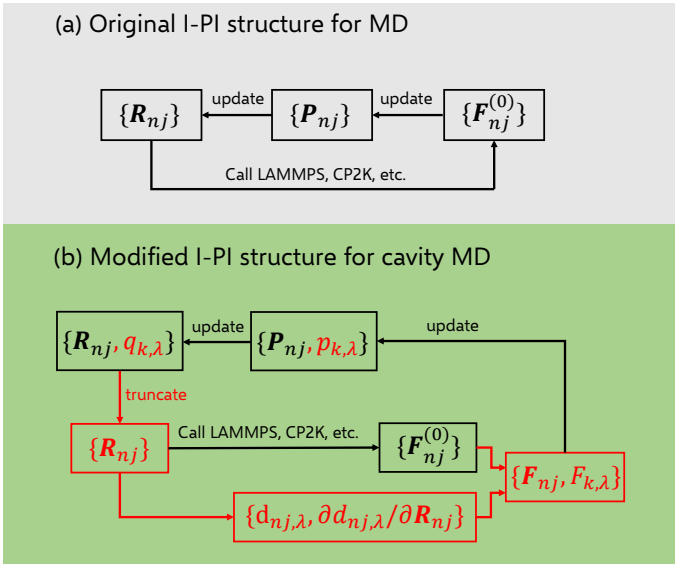

Fig. S1. Illustration of the algorithm structures of (a) the original I-PI for MD simulations and (b) our modified I-PI structure for cavity MD simulations, where the modification is labeled in red.

In the q-TIP4P/F model, the pairwise intermolecular potential is characterized by the Lennard-Jones potential between oxygen atoms plus the Coulombic interactions between partial changes:

$$V^{(nl)}_{\mathrm{inter}} = 4\epsilon\left[\left(\frac{\sigma}{R^{\mathrm{OO}}_{nl}}\right)^{12} - \left(\frac{\sigma}{R^{\mathrm{OO}}_{nl}}\right)^{6}\right] + \sum_{i\in n}\sum_{j\in l}\frac{Q_i Q_j}{R_{ij}} \qquad [S4]$$

where R^{OO}_{nl} denotes the distance between the oxygen atoms and R_{ij} ($i \in n$ and $j \in l$) denotes the distance between the partial charge sites in molecules n and l. Within a single H_2O molecule, two positive partial charge with magnitude $Q_{\mathrm{M}}/2$ are assigned to the hydrogen atoms, and the negatively charge site with magnitude $-Q_{\mathrm{M}}$ is placed at $\mathbf{R}_{\mathrm{M}}$:

$$\mathbf{R}_{\mathrm{M}} = \gamma\mathbf{R}_{\mathrm{O}} + \frac{1-\gamma}{2}\left(\mathbf{R}_{\mathrm{H}_1} + \mathbf{R}_{\mathrm{H}_2}\right) \qquad [S5]$$

For parameters, $\epsilon = 0.1852$ kcal mol^{-1}, $\sigma = 3.1589$ Å, $Q_{\mathrm{M}} = 1.1128\ |e|$ (where e denotes the charge of the electron), and $\gamma = 0.73612$.

The intramolecular interaction is characterized by

$$V^{(n)}_{\mathrm{g}} = V_{\mathrm{OH}}(R_{n1}) + V_{\mathrm{OH}}(R_{n1}) + \frac{1}{2}k_\theta\left(\theta_n - \theta_{\mathrm{eq}}\right)^2 \qquad [S6]$$

where

$$V_{\mathrm{OH}}(r) = D_r\left[\alpha_r^2\left(r - r_{\mathrm{eq}}\right)^2 - \alpha_r^3\left(r - r_{\mathrm{eq}}\right)^3 + \frac{7}{12}\alpha_r^4\left(r - r_{\mathrm{eq}}\right)^4\right] \qquad [S7]$$

Here, R_{n1} and R_{n2} denote the lengths of two O−H bonds, θ_n and θ_{eq} denote the H−O−H angle and the equilibrium angle. For parameters, $D_r = 116.09$ kcal mol^{-1}, $\alpha_r = 2.287$Å^{-1}, $r_{\mathrm{eq}} = 0.9419$Å, $k_\theta = 87.85$ kcal mol^{-1}rad^{-2}, and $\theta_{\mathrm{eq}} = 107.4$ deg.

Given the q-TIP4P/F force field, one can easily calculate the cavity-free force $\mathbf{F}^{(0)}_{nj}$ as a function of the nuclear configurations by standard molecular dynamics packages. The dipole moment is given by

$$\begin{aligned} d_{ng,\lambda} &= \left[\frac{Q_{\mathrm{M}}}{2}\left(\mathbf{R}_{n\mathrm{H}_1} + \mathbf{R}_{n\mathrm{H}_2}\right) - Q_{\mathrm{M}}\mathbf{R}_{n\mathrm{M}}\right]\cdot\boldsymbol{\xi}_\lambda \\ &= \left[\frac{\gamma Q_{\mathrm{M}}}{2}\left(\mathbf{R}_{n\mathrm{H}_1} + \mathbf{R}_{n\mathrm{H}_2}\right) - \gamma Q_{\mathrm{M}}\mathbf{R}_{n\mathrm{O}}\right]\cdot\boldsymbol{\xi}_\lambda \end{aligned} \qquad [S8]$$

and the derivative $\partial d_{ng,\lambda}/\partial\mathbf{R}_{nj}$ is straightforward. In calculating the IR spectrum, the total dipole moment $\boldsymbol{\mu}_S$ is given by $\boldsymbol{\mu}_S\cdot\boldsymbol{\xi}_\lambda = \sum_{n=1}^{N_{\mathrm{sub}}} d_{ng,\lambda}$.

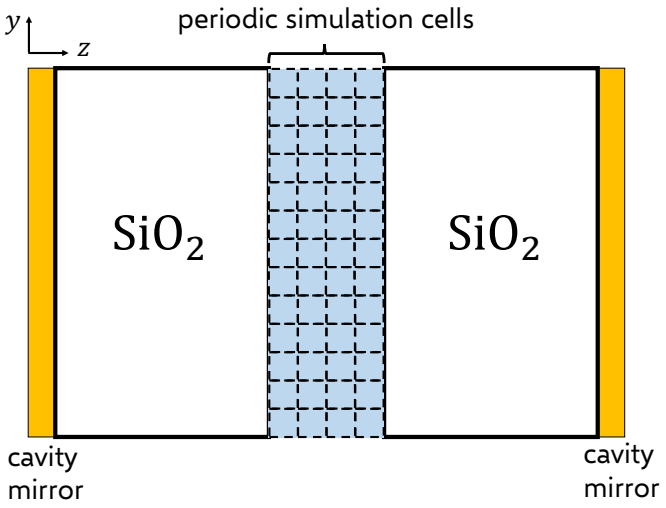

Fig. S2. The structure of the cavity for our simulation. Water molecules are constrained at the center of the cavity by a pair of thick SiO_2 layers.

Implementation Details. We have implemented the above cavity MD scheme by modifying an open-source MD package I-PI (S8), which was designed for both classical and path-integral MD simulations. The general structure of I-PI is illustrated as the gray region in Fig. S1: At every time step, given the molecular positions $\{\mathbf{R}_{nj}\}$, the forces $\{\mathbf{F}^{(0)}_{nj}\}$ were calculated by calling the external package LAMMPS (for classical MD) (S9). The package CP2K (S10) could be used for *ab initio* MD. After calculating the forces, the momenta $\{\mathbf{P}_{nj}\}$ and positions $\{\mathbf{R}_{nj}\}$ are updated accordingly.

Our modification is illustrated as the green region in Fig. S1. We store both the nuclear and photonic degrees of freedom in I-PI. At every time step, we first truncate a nuclear position array $\{\mathbf{R}_{nj}\}$ from the total (nuclear + photonic) position array, and then use the interface of I-PI to calculate the cavity-free forces $\{\mathbf{F}^{(0)}_{nj}\}$. We also calculate the dipole moments and their derivatives from the nuclear position array $\{\mathbf{R}_{nj}\}$. With the cavity-free forces and the dipole moments, we calculate the overall forces on all nuclei and photons $\{\mathbf{F}_{nj}, F_{k,\lambda}\}$ (the right hand side of Eq. (S3)). After calculating the forces, we use the interface of I-PI to update momenta and positions.

Due to the user-friendly structure of I-PI, the current cavity MD code should be easily generalized to the cases of *ab initio* calculation and path-integral cavity MD simulations, results which will be reported in a separate publication.

Simulation Details. We consider the following scenario for simulation. As shown in Fig. S2, the cavity is placed along the z-axis. A pair of thick SiO_2 layers are placed between the cavity mirrors so that the water molecules can move freely only in a small region (but still on the order of microns) near the cavity center. Such additional SiO_2 layers are used (i) to ensure the intermolcular interactions between H_2O molecules are the same as those in free space, and (ii) to validate the long-wave approximation that we have taken from the very beginning. We consider only two cavity modes with polarization directions $\boldsymbol{\xi}_\lambda$ along x and y directions, both of which are resonant with the O−H stretch mode. We set the auxiliary mass for the two photons as $m_{k,\lambda} = 1$ a.u. (atomic units).

2. Simplified 1D Model for V-USC

Starting from the classical Hamiltonian for V-USC (Eq. (S1)), let us assume that (i) the molecules are non-interacting 1D harmonic oscillators, (ii) the dipole moment for a single molecule is linear (i.e., $d_{ng,\lambda} = d_0 x_n$), and (iii) only a single cavity mode is considered. With these simplifications, the Hamiltonian can be written as:

$$H^{\mathrm{G}}_{\mathrm{QED}} = \sum_{n=1}^{N} \frac{p_n^2}{2} + \frac{p_c^2}{2} + V(\{x_n\}, x_c) \qquad \text{[S9a]}$$

where

$$V(\{x_n, x_c\}) = \sum_{n=1}^{N} \frac{1}{2}\omega_0^2 x_n^2 + \frac{1}{2}\omega_c^2 \left(x_c + \frac{2g_0}{\omega_c} \sum_{n=1}^{N} x_n \right)^2 \qquad \text{[S9b]}$$

Here, $g_0 \equiv d_0/2\sqrt{\Omega\epsilon_0}$, and we have assumed all masses to be 1. Note that the self-dipole term (the $\left(\sum_{n=1}^{N} x_n\right)^2$ term in the expanded square above) is necessary for studying V-USC. With the Hamiltonian in Eq. (S9), the equations of motion now read

$$\ddot{x}_n = -\omega_0^2 x_n - 2g_0\omega_c x_c - 4g_0^2 \sum_{l=1}^{N} x_l \tag{S10a}$$

$$\ddot{x}_c = -\omega_c^2 x_c - 2g_0\omega_c \sum_{n=1}^{N} x_n \tag{S10b}$$

Let us define the bright mode as $x_B = \frac{1}{\sqrt{N}} \sum_{n=1}^{N} x_n$, so that the equations of motion for the bright mode and the cavity mode become

$$\ddot{x}_B = -\omega_0^2 x_B - \omega_c \Omega_N x_c - \Omega_N^2 x_B \tag{S11a}$$

$$\ddot{x}_c = -\omega_c^2 x_c - \omega_c \Omega_N x_B \tag{S11b}$$

where $\Omega_N = 2\sqrt{N} g_0$ is the usual Rabi frequency. In the matrix form, the above equations can be written as

$$\ddot{\vec{x}} = -K\vec{x} \tag{S12}$$

where $\vec{x} = (x_B, x_c)^T$ and

$$K = \begin{pmatrix} \omega_0^2 + \Omega_N^2 & \omega_c \Omega_N \\ \omega_c \Omega_N & \omega_c^2 \end{pmatrix} \tag{S13}$$

Note that the Ω_N^2 term above comes from the self-dipole term.

Polariton frequencies. The polariton frequencies ($\omega_\pm$) can be determined by solving the eigenvalues of the matrix K:

$$\omega_\pm^2 = \frac{1}{2}\left[\omega_0^2 + \Omega_N^2 + \omega_c^2 \pm \sqrt{(\omega_0^2 + \Omega_N^2 + \omega_c^2)^2 - 4\omega_0^2\omega_c^2}\right] \tag{S14}$$

At resonance ($\omega_c = \omega_0$), the polariton frequencies are reduced to

$$\omega_\pm^2 = \omega_0^2 + \frac{\Omega_N^2}{2} \pm \Omega_N \sqrt{\omega_0^2 + \frac{\Omega_N^2}{4}} \tag{S15}$$

In the VSC limit ($\Omega_N \ll \omega_0$), Eq. (S15) can be further simplified as

$$\omega_\pm \approx \sqrt{\omega_0^2 \pm \Omega_N\omega_0} \approx \omega_0 \pm \frac{\Omega_N}{2} \tag{S16}$$

which is the usual strong-coupling result.

IR spectrum. The IR spectrum of molecules is calculated by Eq. (5). With our 1D model, the IR spectrum is expressed as

$$n(\omega)\alpha(\omega) \propto \omega^2 \int_{-\infty}^{+\infty} e^{-i\omega t} \langle x_B(0) x_B(t) \rangle \, dt \tag{S17}$$

where we have neglected all prefactors (including the temperature as we take room temperature throughout this manuscript). According to Eq. (S11), the solution of $x_B(t)$ is

$$\begin{aligned} x_B(t) = &\left[x_B(0)\cos^2\left(\frac{\theta}{2}\right) + x_c(0)\cos\left(\frac{\theta}{2}\right)\sin\left(\frac{\theta}{2}\right)\right] e^{i\omega_+ t} \\ &+ \left[x_B(0)\sin^2\left(\frac{\theta}{2}\right) - x_c(0)\cos\left(\frac{\theta}{2}\right)\sin\left(\frac{\theta}{2}\right)\right] e^{i\omega_- t} \end{aligned} \tag{S18a}$$

where

$$\tan(\theta) = 2\omega_c\Omega_N / \left(\omega_0^2 + \Omega_N^2 - \omega_c^2\right) \tag{S18b}$$

By substituting Eq. (S18) into Eq. (S17) and using $\langle x_B(0) x_c(0) \rangle = 0$, we obtain

$$n(\omega)\alpha(\omega) \propto \omega^2 \left[\cos^2\left(\frac{\theta}{2}\right)\delta(\omega - \omega_+) + \sin^2\left(\frac{\theta}{2}\right)\delta(\omega - \omega_-)\right] \tag{S19}$$

The integrated peak areas for LP and UP are

$$I_{\mathrm{LP}} \propto \omega_-^2 \sin^2\left(\frac{\theta}{2}\right) \tag{S20a}$$

$$I_{\mathrm{UP}} \propto \omega_+^2 \cos^2\left(\frac{\theta}{2}\right) \tag{S20b}$$

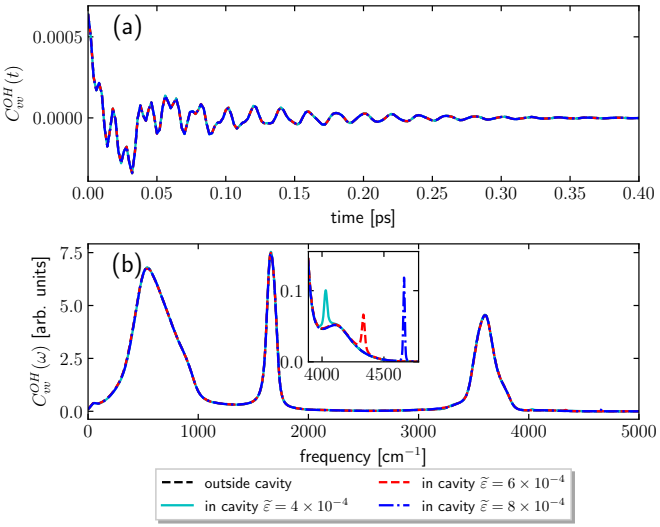

Fig. S3. VACF of O−H bond for individual H_2O molecules plotted in the same manner as Fig. 7. Note that under V-USC, a small side peak also emerges in the spectrum which corresponds to the UP frequency (see the zoom-in insert of Fig. S3b).

From the above, we find that the asymmetric peaks come from two origins: (i) the prefactor $\omega_{\pm}^2$ and (ii) the self-dipole term in the dipole-gauge Hamiltonian. While the first origin is trivial, the second origin can be understood as follows. If we had neglected the self-dipole term, we would naively take $\omega_0^2 + \Omega_N^2 \to \omega_0^2$ in Eq. (S13) and obtain a different expression for θ, $\tan(\theta) = 2\omega_c\Omega_N / \left(\omega_0^2 - \omega_c^2\right)$ (where the Ω_N^2 term now vanishes compared to Eq. (S18b)). At resonance, we would obtain that $\tan(\theta) = \infty$, i.e., $\theta = \pi/2$ and $\cos^2(\theta/2) = \sin^2(\theta/2) = 1/2$. However, because of the Ω_N^2 term, $\theta < \pi/2$, which implies $\sin^2(\theta/2) < \cos^2(\theta/2)$. In other words, when $\omega_c = \omega_0$, the self-dipole term forces the LP to be further suppressed and the UP be further enhanced.

3. Velocity Autocorrelation Function of O−H Bond

We report the VACF of the O−H bond for individual H_2O molecules in Fig. S3, which is plotted in the same manner as Fig. 7. While the VACF of O−H is largely the same for outside (black dashed line) or inside (lines with color) the cavity, we also find a small side peak in the spectrum which corresponds to the UP frequency; see the zoom-in insert of Fig. S3b. However, compared with Fig. S3b, the side peak is much less intense.

4. Multimode Rabi Splitting

The results presented in the manuscript and above are limited to the case of a single-mode cavity. In this section, we consider the case when a multimode cavity is coupled to liquid water. In detail, we consider a cavity of N_m ($N_m > 1$) different cavity modes with frequencies $\omega_{k,\lambda} = m\pi c/L_c(N_m)$ ($m = 1, 2, \cdots, N_m$), where $L_c(N_m)$ denotes the cavity length which depends on N_m. To best isolate and analyze the effect of the multimode cavity, we set the middle cavity mode ($\omega_{k,\lambda} = N_m\pi c/2L_c(N_m)$) at resonance with the O−H stretch mode (with frequency $\omega_0 = 3550$ cm^{-1}) , i.e., the cavity length $L_c(N_m)$ is increased when more cavity modes are considered. Note that when increasing the cavity length, both the cavity volume Ω and the number of simulation cells N_{cell} also increase and with the same proportion. As such, the effective light-matter coupling strength $\widetilde{\varepsilon}_{k,\lambda} = \sqrt{N_{\text{cell}}}\varepsilon_{k,\lambda} = \sqrt{N_{\text{cell}} m_{k,\lambda}\omega_{k,\lambda}^2/\Omega\epsilon_0}$ is kept the same for the middle cavity mode ($\omega_{k,\lambda} = N_m\pi c/2L_c(N_m) = \omega_0$) and one should expect the Rabi splitting for the O−H stretch mode to remain the same as well. Note that, just as for the case of the single-mode cavity, each cavity mode contains two polarization directions (x- and y-direction).

Fig. S4a-d plots the simulated IR spectrum of liquid water coupled to a (a) single-mode, (b) four-mode, (c) six-mode, or (d) ten-mode cavity. The blue lines denote the frequencies of the included cavity modes. Here, the effective light-matter coupling strength for the middle cavity mode is always set as $\widetilde{\varepsilon} = 2 \times 10^{-4}$ cm^{-1}, and as one might expect from the argument above, indeed we do the same Rabi splitting for the O−H stretch mode (~ 3400 cm^{-1}) for each multimode case. Very interestingly, in Fig. S4b (or Fig. S4d), the fundamental cavity mode is resonantly coupled to the H−O−H bending band near 1650 cm^{-1} (or intermolecular librational vibration near 700 cm^{-1}) and an additional Rabi splitting is also observed. As shown in the figure, apart from the Rabi splittings, the decoupled cavity modes can also be found in the IR spectrum. However, the observed frequencies are slightly larger than the cavity modes due to the self-dipole contribution; see Eq. Eq. (S3a). Notably, the intensities of these decoupled cavity peaks can vary significantly.

Fig. S5 plots the IR spectrum of liquid water in the four-mode cavity with different coupling strengths. Compared with the IR spectrum outside the cavity (Fig. S5a), in Fig. S5b-d, increased Rabi splittings for both the O−H stretch mode (~ 3400 cm^{-1}) and the H−O−H bending band (~ 1650 cm^{-1}) are observed when the effective coupling strength $\widetilde{\varepsilon}$ for the

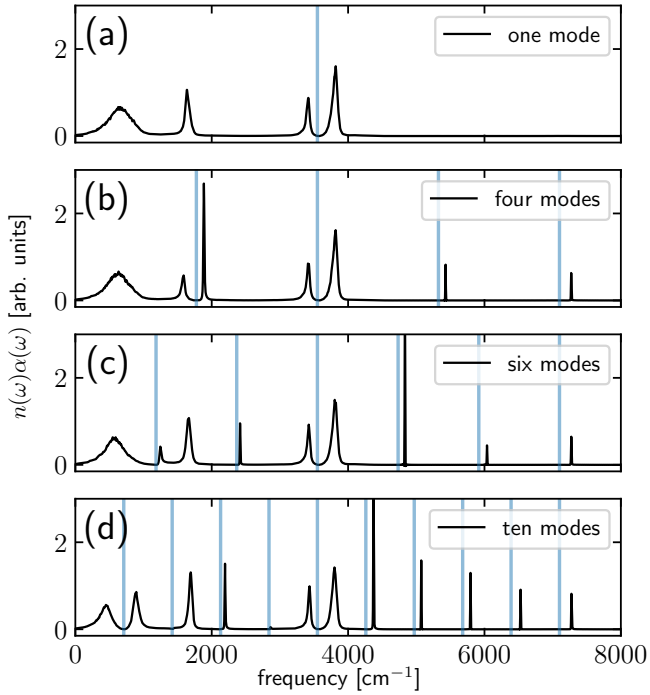

Fig. S4. Simulated IR spectrum of liquid water in a multimode cavity. From top to bottom, we plot the results when a (a) single-mode, (b) four-mode, (c) six-mode, and (d) ten-mode cavity is coupled to liquid water, respectively. The vertical blue lines denote the frequencies of the cavity modes. The effective coupling strength $\widetilde{\varepsilon}$ is always set as 2×10^{-4} a.u. for the middle cavity mode which is resonantly coupled to the O—H stretch mode (~ 3550 cm^{-1}). All other simulation details are the same as Fig. 1. Note that apart from the Rabi splitting for the O—H stretch mode, Fig. S4b (or S4d) also shows the Rabi splitting between the fundamental cavity mode and the H—O—H bending band near 1650 cm^{-1} (or sometimes the intermolecular librational vibration near 700 cm^{-1}). Note that the decoupled cavity modes can also be found in the IR spectrum; however the observed frequencies are slightly larger than those of the cavity modes due to the self-dipole contribution; see Eq. (S3a).

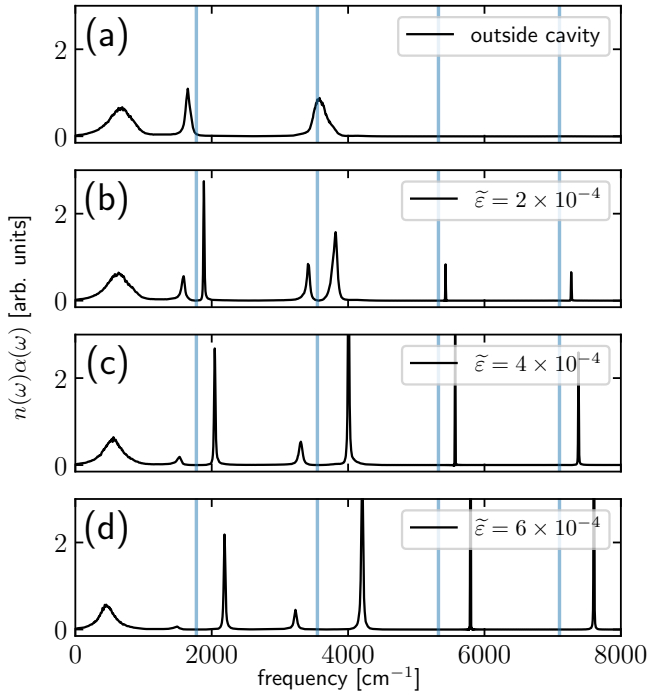

Fig. S5. Simulated IR spectrum of liquid water in a four-mode cavity either (a) outside the cavity; or inside the cavity with effective coupling strength $\widetilde{\varepsilon}$ for the middle cavity mode set as (b) 2×10^{-4}, (c) 4×10^{-4}, and (d) 6×10^{-4} a.u.. The vertical blue lines denote the frequencies of the cavity modes. All simulation details are the same as Fig. S4.

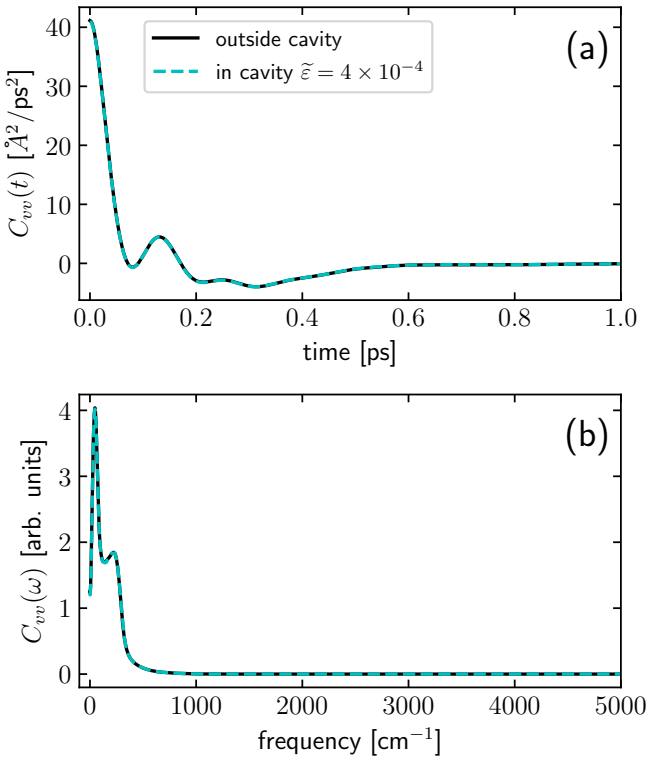

Fig. S6. Velocity autocorrelation function (VACF) of the center of mass of individual H_2O molecules in the four-mode cavity plotted in the same manner as Fig. 6. All simulation details are the same as Fig. S4.

middle photon mode (which is resonantly coupled to the O−H stretch mode) is increased from 2×10^{-4} to 6×10^{-4} a.u..

Finally, we report the VACF for the center-of-mass motion and the orientational autocorrelation function in Figs. S6 and S7 in the same manner as Figs. 6 and 7. Clearly, for a multimode cavity, the center-of-mass VACF is not changed, but the orientational autocorrelation function is slightly modified, similar to what was reported in Fig. 7 of the main text for the single-mode case.

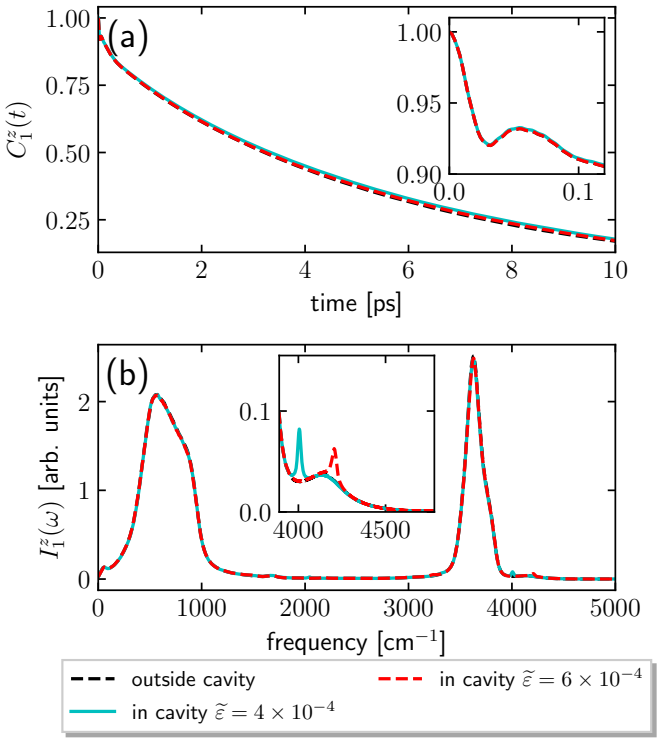

Fig. S7. z-component of first-order orientational autocorrelation function (OACF) of individual H_2O molecules in the four-mode cavity plotted in the same manner as Fig. 6. All simulation details are the same as Fig. S4.

[S1] Tuckerman M (2010) *Statistical mechanics: theory and molecular simulation.* (Oxford University Press, New York).
[S2] Markland TE, Ceriotti M (2018) Nuclear quantum effects enter the mainstream. *Nat. Rev. Chem.* 2(3):0109.
[S3] Thomas A, et al. (2016) Ground-State Chemical Reactivity under Vibrational Coupling to the Vacuum Electromagnetic Field. *Angew. Chemie Int. Ed.* 55(38):11462–11466.
[S4] Lather J, Bhatt P, Thomas A, Ebbesen TW, George J (2019) Cavity Catalysis by Cooperative Vibrational Strong Coupling of Reactant and Solvent Molecules. *Angew. Chemie Int. Ed.* 58(31):10635–10638.
[S5] Hiura H, Shalabney A, George J (2018) Vacuum-Field Catalysis: Accelerated Reactions by Vibrational Ultra Strong Coupling. *ChemRxiv. Preprint.* https://doi.org/10.26434/chemrxiv.7234721.v4.
[S6] Thomas A, et al. (2019) Tilting a ground-state reactivity landscape by vibrational strong coupling. *Science* 363(6427):615–619.
[S7] Habershon S, Manolopoulos DE (2009) Zero point energy leakage in condensed phase dynamics: An assessment of quantum simulation methods for liquid water. *J. Chem. Phys.* 131(24):244518.
[S8] Kapil V, et al. (2019) i-PI 2.0: A universal force engine for advanced molecular simulations. *Comput. Phys. Commun.* 236:214–223.
[S9] Plimpton S (1995) Fast Parallel Algorithms for Short-Range Molecular Dynamics. *J. Comput. Phys.* 117(1):1–19.
[S10] Hutter J, Iannuzzi M, Schiffmann F, VandeVondele J (2014) Cp2k: atomistic simulations of condensed matter systems. *Wiley Interdiscip. Rev. Comput. Mol. Sci.* 4(1):15–25.